Angular distribution of different vibrational components of the X and B states reached after resonant Auger decay of core-excited H_2O: Experiment and theory

I. Hjelte, L. Karlsson, and S. Svensson
Department of Physics, Uppsala University, S-75121 Uppsala, Sweden

A. De Fanis
Institute of Multidisciplinary Research for Advanced Materials, Tohoku University, Sendai 980-8577, Japan and Japan Synchrotron Radiation Research Institute, Sayo-gun, Hyogo 679-5198, Japan

V. Carravetta
IPCF-CNR, via Moruzzi 1, 56124 Pisa, Italy

N. Saito
National Institute of Advanced Industrial Science and Technology, Tsukuba 305-8568, Japan

M. Kitajima and H. Tanaka
Department of Physics, Sophia University, Tokyo 102-8554, Japan

H. Yoshida and A. Hiraya
Department of Physical Science, Hiroshima University, Higashi-Hiroshima 739-8526, Japan

I. Koyano
Department of Material Science, Himeji Institute of Technology, Kamigori 678-1297, Japan

K. Ueda
Institute of Multidisciplinary Research for Advanced Materials, Tohoku University, Sendai 980-8577, Japan

M. N. Piancastelli
Department of Physics, Uppsala University, S-75121 Uppsala, Sweden and Department of Chemical Sciences and Technologies, University "Tor Vergata", 00133 Rome, Italy

(Received 29 October 2004; accepted 1 December 2004; published online 15 February 2005)

Vibrationally resolved spectra have been obtained for the lowest-lying cationic states X $^2B_1$, A $^2A_1$, and B $^2B_2$ of the water molecule reached after participator resonant Auger decay of core-excited states. The angular distribution has been measured of the first four vibrational components of the X state in the photon energy regions including the O $1s \rightarrow 4a_1$ and the O $1s \rightarrow 2b_2$ core excitations, and for different portions of the vibrational envelope of the B state in the photon energy region including the O $1s \rightarrow 2b_2$ core excitation. For the X state, a large relative spread in β values of the different vibrational components is observed across both resonances. For the B state, a very different trend is observed for the high binding energy side and the low binding energy side of the related spectral feature as a function of photon energy. A theoretical method based on the scattering K matrix has been used to calculate both the photoabsorption spectrum and the β values, by taking both interference between direct and resonant photoemission and vibrational/lifetime interference into account. The numerical results show qualitative agreement with the trends detected in the experimental values and explain the conspicuous variations of the β values primarily in terms of coupling between direct and resonant photoemission by interaction terms of different sign for different final vibrational states. © *2005 American Institute of Physics*. [DOI: 10.1063/1.1850898]

I. INTRODUCTION

The water molecule has been extensively studied largely because of its relative simplicity and biological importance. The electron configuration of the ground state is well established and can be written as

$$1a_1^2 2a_1^2 1b_2^2 3a_1^2 1b_1^2 ({}^1A_1),$$

where $1a_1$ corresponds to the O 1s orbital and $2a_1$ is largely due to the O 2s orbital. The $1b_1$ orbital is mainly associated with the out-of-plane O $2p_x$ atomic orbital while $1b_2$ and $3a_1$ are mainly in-plane O $2p_y$ and O $2p_z$ orbitals in antisymmetric and symmetric, respectively, combination with the H 1s orbitals.

Despite all efforts, there is still much more to learn about this molecule. High-resolution synchrotron facilities permit the observation of vibrational structures for cationic states reached via resonant Auger transitions. In particular, studies of the photon energy and angular dependence of the vibrational excitations provide a wealth of new information about the photoionization process and the electronic structure of the molecule.

Early studies of angular distributions of photoejected

electrons from atoms and molecules concerned photoionization of valence electrons in the direct ionization and autoionization regions.[1,2] By using synchrotron radiation and beamline techniques the studies have been extended to inner-shell photoemission[1,3] and resonant Auger emission.[4,5] Few studies focus on resonant Auger emission of molecules and have been carried out for Cl_2,[6] CO,[7] HCl,[8,9] and N_2.[10] Investigations of angular distributions involving individual vibrations within a resonant Auger final state have so far only been performed on CO.[11,12] A photon energy dependence of the angular distribution of different vibrational states has been observed for CO when exciting to different intermediate states.[12] In vibrationally resolved measurements on CO (Ref. 11) it has been found that the angular distribution varies between different vibrational final states. This behavior was attributed mainly to contributions from direct photoionization, but no explicit theoretical analysis was presented.

For valence studies, it is well known that the variation of the angular distribution as a function of photon energy can be substantially influenced by autoionization processes.[13–17] The reason is that the autoionization resonance causes different enhancement and phase shift of different contributions to the complex amplitude of the relevant photoionization channel.[18–20] We will show that this is also the case for the resonant Auger emission involving the core excitation. Moreover, it is expected that resonant Auger emission show different angular anisotropy from normal Auger emission. The angular anisotropy should be larger in the resonant Auger case, where only one electron carries away angular momentum, in contrast with the normal Auger case where the initial photoelectron can carry away some of the anisotropy of the excitation process.[4,21–23] The lifetime of the core-excited state as well as vibrational/lifetime and direct-resonant path interference effects may also affect the angular distribution of resonant Auger emission.[11]

It is worth to note the following with some relevance to the present study.

In studies of rare gas atoms[4,24–27] and metal vapor atoms,[28,29] the angular anisotropy of resonant Auger electrons has been found to be strongly affected by many-electron interactions. For C_2H_2, it has been found that the nature of the excited orbital influences the angular distribution even when the symmetries of the states involved are alike.[30] A similar effect has been noted for HCl, where the angular distribution from two different intermediate states having the same symmetry was found to differ.[31]

In the present study, we have recorded vibrationally resolved resonant Auger electron spectra of H_2O on and around the O $1s \rightarrow 4a_1$ and $\rightarrow 2b_2$ resonances. The O $1s \rightarrow 4a_1$ resonance is dissociative on a femtosecond time scale[32] whereas the O $1s \rightarrow 2b_2$ resonance is more long lived. It displays vibrational structure at low excitation energies[33] but there are indications that it may become dissociative at higher excitation energies.[34] The final states considered are the first three participator decay states corresponding to the $X(1b_1^{-1})$, $A(3a_1^{-1})$, and $B(1b_2^{-1})$ cationic states. The measurements have been performed at 0° and 90° relative to the polarization plane of the photons. From these data we have been able to extract information concerning the angular distribution of the emitted Auger electrons.

In order to analyze some of the experimental data we have proposed a theoretical one-step model to describe the resonant Auger angular distribution, taking into account both the vibrational/lifetime interference and the interference between direct and resonant photoemission. The calculations are shown to reproduce qualitatively the main trends with the photon energy observed in the β values.

II. EXPERIMENTAL METHODS

The data were acquired at beamline 27SU at SPring-8 using a figure-8 type undulator producing horizontally and vertically polarized light at different overtones.[35,36] The light is monochromatized using a variable line-space plane grating.[37] The polarization was determined from a separate experiment[38] and it was found that it was not entirely linear for the present condition of the large acceptance angles of the photon beam. The degree of polarization is estimated for the 90° and 0° polarization as 0.95 ± 0.05 and 0.82 ± 0.02. This was accounted for in the procedure to determine the β values.

The electron spectrometer is a high-resolution Scienta SES-2002 instrument employing a hemispherical electron energy analyzer. The lens and entrance slit system of the spectrometer are placed in the horizontal plane: the entrance slit is parallel to the incoming photon beam direction while the lens axis is perpendicular to it. The resulting linewidth in the resonant Auger spectra of H_2O was about 0.14 eV.

These experiments were performed under resonant Raman conditions, which means that the incident photon energy distribution, 100 meV full width at half maximum (FWHM), is narrower than the lifetime width of the excited state, 155 meV FWHM. Since the resonant Auger electron energy distribution is determined by the product of the photon energy distribution and the lifetime broadening of the excited state, subnatural lifetime widths may be obtained. Also, it allows one for scanning different parts of the excited state potential energy surface.

There may be sources of error that would affect the results presented below. When changing the angle between the polarization plane of the photons and the spectrometer, there is a change in the photon energy that needs to be compensated for. Changing the direction of polarization can be done by changing the undulator gap and selecting a different overtone, without changing the settings of the monochromator and the electron spectrometer. Changing the undulator gap however causes the change of heat load for the optics and the temperature of the grating changes. This causes the change, of the order of tens of meV, in photon energy passing through the monochromator. To compensate for this energy shift, we frequently recorded the ion yield spectrum, before and after recording the electron spectra, as well as in between. For this ion yield measurement, we have used a total-ion detector located upstream the electron spectrometer at the beamline.[39] Also, by checking the energy of the participator Auger electrons of each recorded spectrum *in situ*, we have

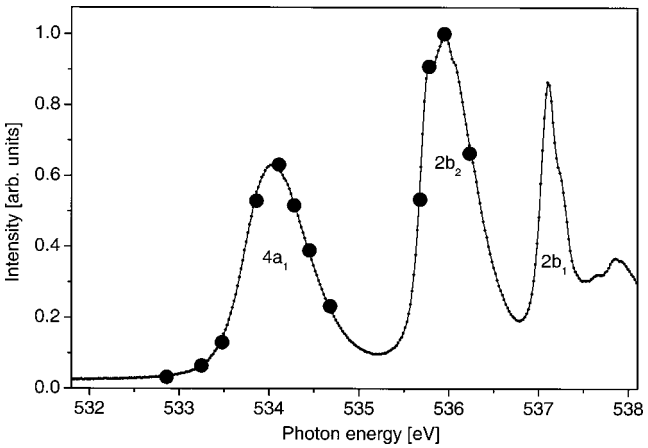

FIG. 1. Absorption spectrum of H_2O measured in the partial electron yield mode below the O 1s ionization threshold. The dots indicate the photon energies at which resonant Auger spectra have been obtained.

confirmed that the photon energy is indeed the one we set. Whenever we found the energy shift in the electron spectrum, we compensated it by adjusting the photon energy so that the electron kinetic energy coincides with the one we want. We know from several investigations that by this procedure the photon energy in any given electron spectrum is constant within ±20 meV at most.

III. EXPERIMENTAL RESULTS

Figure 1 shows the total ion yield of H_2O measured over the O $1s \rightarrow 4a_1$, $\rightarrow 2b_2$, and $\rightarrow 2b_1$ resonances. The photon energy scale has been calibrated by comparison with previous measurements.[33] The photon energy values at which electron decay spectra have been obtained are marked by dots. Figure 2 shows the resonant Auger spectra taken with horizontally and vertically polarized radiation tuning over the $4a_1$ and $2b_2$ intermediate states. The photon energies used for this figure are marked in the partial electron yield spectrum in Fig. 1. The three spectral structures originate from participator decay involving the three lowest-lying single-hole states X $1b_1^{-1}\,{}^2B_1$, A $3a_1^{-1}\,{}^2A_1$, and B $1b_2^{-1}\,{}^2B_2$. Figure 3 shows the enlarged off- and on-resonance spectra for both intermediate states. The spectra have been normalized to the intensity of the first vibrational peak associated with the O $1s \rightarrow 2b_2$ spectrum obtained for horizontal polarization. As can be seen, the participator decay to the $1b_1^{-1}$ final state is accompanied by extended vibrational structure while tuning over both resonances. In contrast, the $3a_1^{-1}$ state resonates when the photon energy is on top of the O $1s \rightarrow 4a_1$ intermediate state while the $1b_2^{-1}$ final state is greatly enhanced on the O $1s \rightarrow 2b_2$ resonance.

Excitations of the O–H symmetric stretching vibrational mode ν_1 are clearly observed for the outermost $1b_1^{-1}$ final state. The number of quanta increases across both resonances, which suggests that the molecular equilibrium geometry of the core-excited state differs from that in the final state. In Fig. 4, we present a high-resolution resonant Auger spectrum of the $1b_1^{-1}$ final state, taken at a photon energy, 535.95 eV,[33] tuned to the top of the O $1s \rightarrow 2b_2$ resonance. The vibrational progression associated with the ν_1 symmetric

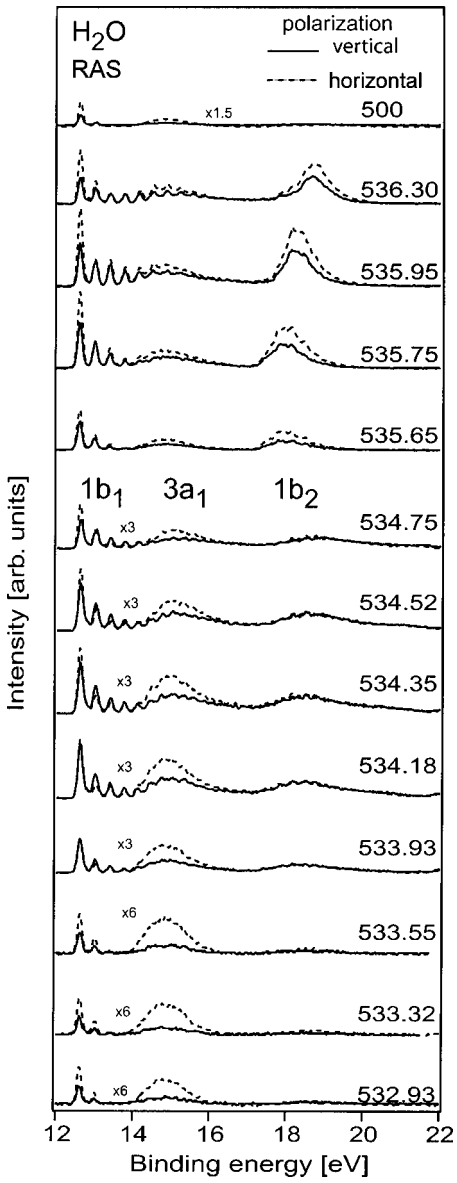

FIG. 2. Resonant Auger spectra measured with horizontally (dotted line) and vertically (solid line) polarized radiation. The photon energy values correspond to the positions marked in Fig. 1.

stretching normal mode, which consists of only four peaks in direct photoemission,[40] extends over a wide energy range and crosses the broad peak associated to the $3a_1^{-1}$ final state. In addition to the progression from the ν_1 mode, one can observe some weak lines originating from the ν_2 bending mode. Very few vibrational modes can be seen for this latter mode, which implies that the molecule does not bend much in the intermediate core-excited state. The extended ν_1 symmetric stretching mode on the other hand shows that the molecule exhibits much dynamical behavior during the same short (a few femtoseconds) time interval.

The energies of the ν_1 progression are shown in Table I. The vibrational constants, obtained by fitting a parabolic polynomial in $(\nu+1/2)$ to these data, are $\omega_e = 0.4064$ eV and $\omega_e x_e = 0.0043$ eV. These values are slightly larger than the values $\omega_e = 0.396$ eV and $\omega_e x_e = 0.0039$ eV obtained from IR measurements,[41] but rather close to previous values from UV-photoelectron spectroscopy.[40] The discrepancies may be

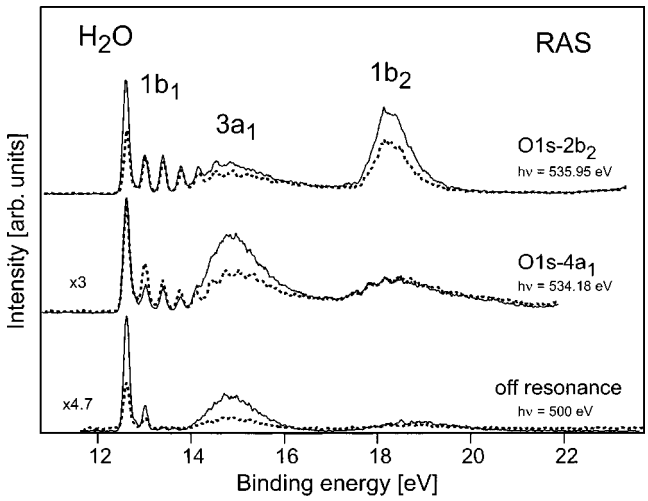

FIG. 3. Off- resonance spectrum and on-resonance spectra obtained at photon energies corresponding to the top of the O $1s \rightarrow 4a_1$, O $1s \rightarrow 2b_2$ intermediate states, respectively, with horizontal polarization (solid line) and vertical polarization (dotted line). The spectra have been normalized to the intensity of the first vibrational peak obtained for horizontal polarization.

explained by the uncertainty in the line positions in the electron spectra due to the extensive rotational substructure. Another source of uncertainty is the presence of the $3a_1^{-1}$ state in the case of the higher vibrational components.

We have studied the angular dependence of the first four vibrations of the $1b_1^{-1}$ final state and used the well-established equation

$$\frac{d\sigma}{d\Omega} = \frac{\sigma_{\text{total}}}{4\pi}\left[1 + \frac{\beta}{4}(3P\cos 2\theta + 1)\right] \quad (1)$$

to obtain the photoelectron asymmetry parameter β.[42]

In this expression, $d\sigma/d\Omega$ is the differential cross section, θ is the angle between the detected electron and the plane of the radiation, and P is the degree of plane polarization. For the 90° and 0° directions, values of P are 0.82 and 0.95, respectively.[38] In order to obtain the relative intensities of the structures, a linear background has been subtracted from the data. In addition, the fitting procedure included a region containing a large portion of the $3a_1^{-1}$ final state in order to remove direct contributions to the intensity arising from this state. The first four vibrational peaks were fitted under the assumption that the vibrational energy separations are identical to those in Table I for each resonant Auger transition.

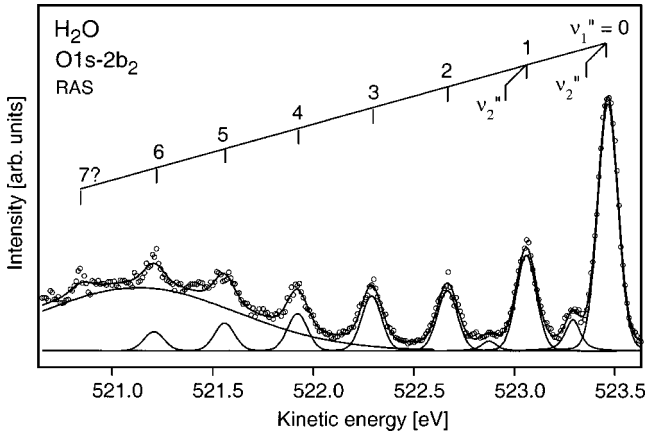

FIG. 4. High-resolution resonant Auger spectrum of the $X(^1b_1^{-1})$ state, obtained at a photon energy of 535.95 eV, corresponding to the maximum of the O $1s \rightarrow 2b_2$ resonance.

TABLE I. Vibrational energies in the resonant Auger (participator) electron band of the $X(1b_1^{-1})$ final state.

Vibrational quantum number	Binding energy (eV)
0	12.622
1	13.029
2	13.420
3	13.797
4	14.166
5	14.528
6	14.879
7	15.240

The resulting photoelectron asymmetry parameter for the $1b_1^{-1}$ final state, obtained at several points across the O 1s $\rightarrow 4a_1$ and $\rightarrow 2b_2$ resonances, is shown in Fig. 5. Apparently, there is a large variation in the asymmetry for the different vibrational components. All vibrations except (0,0,0) have a low β value across each resonance, in particular for the O $1s \rightarrow 4a_1$ resonance, where most values are negative. For

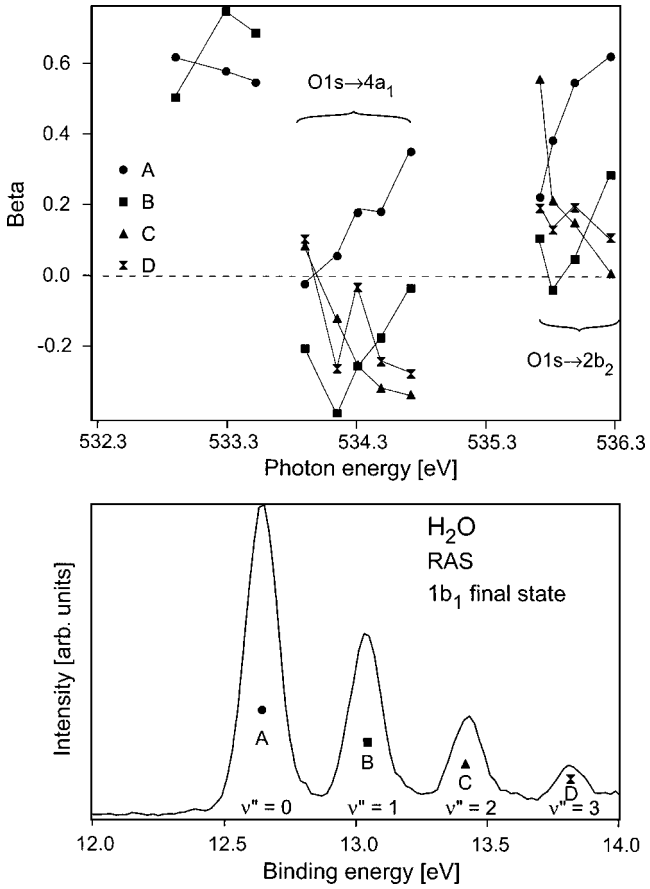

FIG. 5. Top: asymmetry parameter β derived for the first four vibrational components A, B, C, and D of the $X(^1b_1^{-1})$ state in the photon energy region including the O $1s \rightarrow 4a_1$ and O $1s \rightarrow 2b_2$ resonances. Bottom: resonant Auger spectrum for the $X(^1b_1^{-1})$ state, showing the symbols used in the top part for the first four vibrational peaks.

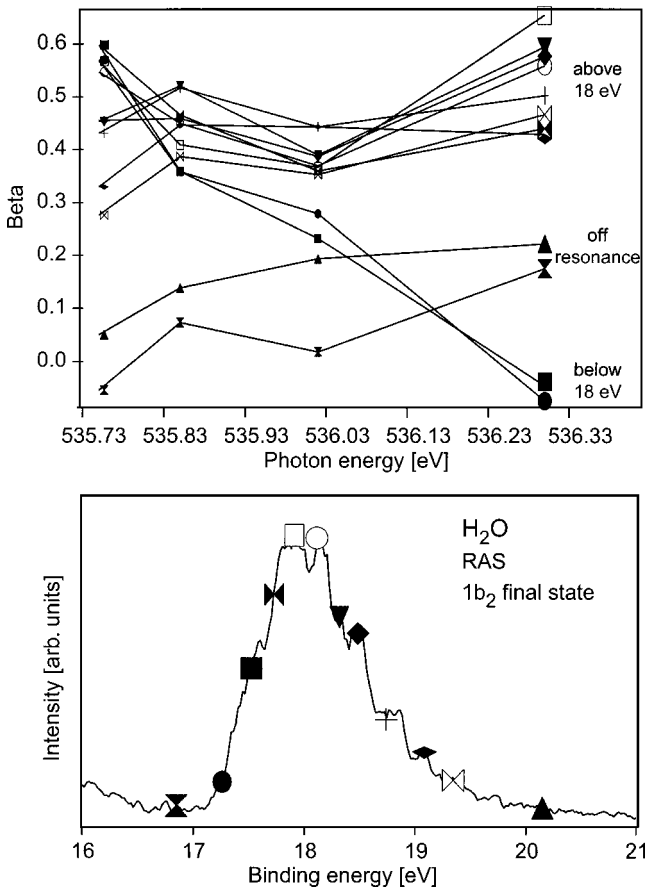

FIG. 6. Top: asymmetry parameter β derived for several portions of the spectral feature related to the $B(1b_2^{-1})$ state (see text) in the photon energy region of the O $1s \rightarrow 2b_2$ resonance. Bottom: resonant Auger spectrum for the $B(1b_2^{-1})$ state, showing the symbols used in the top part for the different portions of the peak.

the first vibration (0,0,0), β is essentially positive and seems to increase gradually with increasing photon energy. This deviating behavior may be due to a contribution from direct photoionization and even interference effects as previously observed for the photoionization branching ratios of neon,[43,44] argon,[45,46] and CO,[47] where the relative intensities of some final states displayed marked differences when tuning the photon energy on and around the core excitation resonance.

There is also a large variation of the intensity of the $1b_2^{-1}\,{}^2B_2$ final state as the photon energy is tuned across the O $1s \rightarrow 2b_2$ resonance. The shape of the band changes, with the center of gravity of the structure shifting towards higher binding energy, as the photon energy is increased (see Fig. 2). The photoelectron asymmetry parameter obtained for this state is shown in Fig. 6. Since this band is not clearly vibrationally resolved, the asymmetry parameter was obtained by dividing the structure into several different binding energy sections and taking the area of each section. The center of each section is marked in the figure. As can be seen, for binding energies below 18 eV, β varies with the photon energy in a remarkable different manner than for the higher binding energies.

As seen in Fig. 2, the electron emission associated with the $1b_2^{-1}$ final state is apparently isotropically distributed in the off-resonance spectrum as well as when tuning over the $4a_1$ intermediate state. This is, however, not the case when tuning over the $2b_2$ intermediate state. There is a very clear dependence on the intermediate state.

There are several sources of error which can affect the determination of the β values for the different vibrational components of the $1b_1$ state. To compensate for the influence of the neighboring and partially overlapping spectral feature related to the $3a_1$ final state, an extended region including this final state has been used in the curve fitting of the $1b_1$ final state as can be seen in Fig. 4. This is done so that the background can be properly determined. The effect is strongest for the v4 peak but also the v3 is affected on top of the O 1s to $4a_1$ and $2b_2$ resonances. The uncertainty is therefore higher for these two final state vibrations.

The first three components of the bending mode vibrational substructure are included in the fitting. As these are well known from previous works[40] their position as well as intensity can be very well accounted for and therefore induce a negligible error in the determination of β for the stretch mode vibrations.

Any difference in efficiency due to, e.g., beam position at the two different polarization angles can be discovered by performing normal Auger at the two angles, normalizing to the intensity of the radiation, and comparing the two spectra. This provided a value of a 2% difference between the polarizations.

The largest source of error in the calculation of the photoelectron asymmetry parameter originates in the determination of the partial cross sections of the features studied. To estimate the error for the $1b_1$ final state a fitting routine has been used allowing an extraction of the standard deviation for each parameter used in the original fitting of each spectrum. This gives an error that is on the order of 10% for the different fitted peaks, where the features with a low signal to background ratio are a bit higher while the on-resonance features are lower. The final error in the determination of the β parameter then is on the order of ±15%. If this is applied to the graph of the $1b_1$ final state in Fig. 5 it is clear that the general trends of the variation in the β parameter remains the same.

Determining the error for the $1b_2$ final state is more difficult as the β parameter was found by observing how different areas of the spectral structure changed with the photon energy. Here the error is most likely larger than for the $1b_1$ final state but this still cannot explain the differences in behavior below and above 18 eV binding energy as seen in Fig. 6.

IV. THEORETICAL METHODS AND RESULTS

In the Born–Oppenheimer approximation the vibronic [Ψ (electronic), χ (vibrational)] wave functions for the ground, the intermediate (resonant), and the final (continuum) states of a resonant photoemission process in a molecule can be written, respectively, as

$$|g,0\rangle = |\Psi_g\rangle|\chi_0^g\rangle \quad \text{(ground)}, \tag{2}$$

$$|r,i\rangle = |\Psi_r\rangle|\chi_i^r\rangle \quad \text{(resonant)}, \tag{3}$$

$$|f,j\rangle = |\Psi_f\rangle|\chi_j^f\rangle \quad \text{(final)}. \tag{4}$$

Following the Franck–Condon (FC) principle, we will write the dipole transition moments for transitions from the ground state to the final and the resonant state, respectively, as

$$\langle g,0|\hat{r}|f,j\rangle \sim \langle \Psi_g|\hat{r}|\Psi_f\rangle_{r,R_0}\langle \chi_0^g|\chi_j^f\rangle_R = t_f F_{0j}^{gf}, \tag{5}$$

$$\langle g,0|\hat{r}|r,i\rangle \sim \langle \Psi_g|\hat{r}|\Psi_r\rangle_{r,R_0}\langle \chi_0^g|\chi_i^r\rangle_R = t_r F_{0i}^{gr}, \tag{6}$$

and the Coulomb coupling between resonant and final continuum states as

$$\langle r,i|\hat{H}|f,j\rangle \sim \langle \Psi_r|\hat{H}_{\text{elec}}|\Psi_f\rangle_{r,R_0}\langle \chi_i^r|\chi_j^f\rangle_R = V^r{}_f F_{ij}^{rf}, \tag{7}$$

where t is an electronic transition dipole moment and F is an overlap between vibrational wave functions. In Eqs. (5)–(7) the subscripts r and R indicate that the integrations are performed, respectively, on the electronic and nuclear coordinates, while R_0 indicates that the nuclear coordinates are fixed at the equilibrium geometry of the ground state. The assumption of a negligible dependence from the nuclear geometry in the FC region is well justified, in the present context, both for t and V.[48]

The amplitude for the direct photoemission process (away from any resonance) is proportional to $t_f F_{0j}^{gf}$. For the calculation of the angular distribution parameter β, the electronic final state in the continuum $|\Psi_f\rangle$ is conveniently decomposed in partial waves and β is obtained as a ratio of linear combinations of dipole transition moments between ground state and partial waves, i.e., a linear combination of partial waves amplitudes.[49] For a given final vibrational state $|\chi_j^f\rangle$, the vibrational factor F_{0j}^{gf} is the same for each one of these dipole transition moments; as a consequence it does not affect the ratio and thus β, in the Born–Oppenheimer approximation, results to have the same value for each final vibrational state. In the case of high photoelectron energy, for instance for photon energies in the region of core excitations, the dipole transition moments for valence ionization have a weak energy dependence. The β parameter for direct valence ionization is almost constant, in a range of a few eV, for high photon energies away from the resonance.

The situation is different in the case of valence resonant photoemission, e.g., at photon energies close to that of a core-excited state, because a resonant amplitude adds to and can interfere with the direct amplitude of Eq. (5). The resonant amplitude that can be shortly written as

$$\frac{t_r F_{0i}^{gr} V^r{}_f F_{ij}^{rf}}{\omega - \omega_{ri} + i\Gamma} \tag{8}$$

for a single vibronic resonance,[47] has evidently a vibrational factor different from that of the direct amplitude in Eq. (5), and it is strongly energy dependent by the denominator, where ω is the photon energy, $\omega_{ri}=E_{ri}-E_{g0}$ is the excitation energy and Γ the linewidth of the vibronic core-excited state.

Considering that the resonant amplitude on top of a core resonance is typically 10–100 times larger than the direct amplitude, its contribution to the total photoemission amplitude, despite the decreasing factor due to the denominator, can remain relevant in an energy region around the resonance as large as several times the linewidth of the resonance. The direct and resonant amplitudes add up with positive interference on one side of the resonance and negative interference on the other side; this gives origin to the well known asymmetry of the resonant photoemission (Fano) profile.[18] The deviation from the symmetric (Lorentzian) profile obtained by neglecting the direct term is rather small but it may lead, anyway, to a relevant energy dependence of the valence photoemission branching ratios, as was proved by an experimental and theoretical investigation on resonant photoemission around a core-excited state of CO (Ref. 47) and recently recognized also for atoms,[43,44] following the pioneer measurements on Ar.[45]

We already pointed out that, as well as the ionization branching ratios, the β parameter is given by a ratio of linear combinations of partial waves amplitudes. Depending on symmetry selection rules, some of these amplitudes will have a resonant, energy dependent contribution for photon energies around the core excitation, giving origin to an energy dependent β. Again, as in the case of the branching ratios, it is the presence of a ratio in the expression of the molecular properties, the anisotropy parameter in the present case, which amplifies the effect of the interference between direct and resonant amplitude. Therefore β, which is practically constant for photon energies far away from the core resonance where the direct ionization is dominant, turns out to be strongly energy dependent for detunings from the resonance as large as 1 eV, where the resonant contribution to some partial wave amplitudes still remains larger or comparable to the direct contribution.

In order to verify quantitatively the hypothesized effect on β of both vibrational/lifetime interference and interference between direct and resonant photoemission, we considered a one-step theoretical model for resonant photoemission including one or two ($i=1,2$) vibronic states corresponding to the same electronic core resonance (r) merged in the high energy continua (different partial waves) due to the ionization of a valence shell f leaving the molecule in a specific vibrational state j. The interaction of a number of discrete states and a number of continua can be conveniently described, from a computational point of view, by a theoretical method based on the scattering K-matrix approach projected on a basis set, which has already been extensively applied to the simulation of molecular photoionization in the low energy region.[49,50] The main quantities needed for such a simulation are the electronic and vibrational matrix elements in Eqs. (5)–(7). The electronic quantities at fixed ground state geometry, namely, core excitation energy (E_r-E_g), valence ionization potential (E_f-E_g), resonant (t_r) and final (t_f) dipole transition moments, Coulomb coupling (V_{rf}) and partial wave phase shifts, have been computed *ab initio* for H_2O in the static-exchange approximation by a one-center expansion on a basis set of L^2 functions[49] (STOCOS) that, having an oscillating factor, are particularly efficient for the description of continuum states even in the high energy region considered here.[51,52] In the calculation the core-excited state O 1s $\rightarrow 2b_2$ and the valence ionization channel $1b_1^{-1}$ were considered. In what concerns the vibrational quantities, we avoided computationally demanding calculations that would be be-

yond the scope of the present theoretical model of resonant photoionization, and adopted reasonable values for the vibrational energy of the resonant state and for the vibrational overlaps F that must be seen as parameters that make the model valid in a wider context. For the factors F in Eqs. (5)–(7) we made the assumption, justified by the different nodal structure of the vibrational functions, that, even for the same final electronic state, they may have a different sign for different vibrational resonant states i. It can be pointed out that the occurrence of vibrational overlaps of opposite sign in the resonant photoionization of CO by decay from different vibrational levels of the C $1s \rightarrow \pi^*$ state has been verified experimentally in a recent investigation,[11] where the vibrational/lifetime interference, but not the interference between direct and resonant path, was explicitly considered in the interpretation of the large variations observed in the anisotropy parameter. As will be shown in the following section, the relative sign of factors F, more than their effective absolute value, is relevant in the modulation of β for photon energies close to the vibrational resonances by a complex mechanism including both types of interference effects.

V. DISCUSSION

In the present experiment, the final states are the same, but with changing photon energy we reach these final states via different intermediate states. As the present results show (see, e.g., Figs. 2 and 3, in particular, what concerns the $1b_2^{-1}$ final state), different intermediate states result in different angular distributions of the emitted electrons. We deal with two intermediate states of different character, one (O $1s \rightarrow 4a_1$) is dissociative on an ultrafast time scale and the other (O $1s \rightarrow 2b_2$) is bound, perhaps becoming dissociative at higher energies. The substantial differences in the angular distributions of the emitted electrons, in particular of the $1b_2^{-1}$ final state, can be attributed to the intermediate states.

It is well known that there is a selectivity that comes into play in the core excitation process, since the linearly polarized light will be preferably absorbed by those molecules having the excited orbital aligned to the polarization axis. A core excitation tends to produce an excited molecule with a definite symmetry and orientation[42] and the angular dependence of the excitation can be measured using angular resolved ion yield measurements. Auger decay also contains its own angular distribution that depends on the symmetry of the final state. The angular distribution of the emitted electron in resonant Auger decay would then reflect both these effects. Knowing this, it has been proposed to calculate the angular dependence of the Auger decay using the simple expression

$$\beta = \beta_m c_a, \tag{9}$$

where β_m is an alignment parameter describing the asymmetry of the molecular orientation following photoabsorption while c_a is the asymmetry of the Auger decay.[29] This relationship was originally derived for cylindrically symmetric molecules and a prerequisite is that the excitation and deexcitation processes can be completely separated (two-step process). In the present case of resonant Auger deexcitation, instead of normal Auger decay, of a triatomic molecule, Eq. (9) may not be applied in a straightforward way. In fact, the measured values of asymmetry parameters change across the resonance, whereas Eq. (9) predicts a constant value for a resonance.

There can be several reasons for this, the most obvious is that a resonant Auger process may not be described as a two-step process, i.e., the basic assumption of Eq. (9). It can be noted that Kukk *et al.*[11] have reported unphysical values of c_a in the case of CO. This molecule is cylindrically symmetric and one might therefore suggest that it is mainly the "one-step" character of the resonant Auger process that makes Eq. (9) not valid: they ascribed the breakdown of the two-step model to the contribution from the direct photoionization, as well as the vibrational/lifetime interference.

We need then to analyze the present experimental data adopting a more sophisticated one-step theoretical model that describes correctly the symmetry of H_2O and that includes both vibrational/lifetime interference and interference between direct and resonant photoemission; this was done by the calculations described in the preceding section. The proposed model has a general validity but let us consider it focused on the interpretation of the energy dependence of β for the $1b_1^{-1}$ channel in the region of the O $1s \rightarrow 2b_2$ resonance, because in this case different final vibrational states are very well resolved, as shown in Fig. 4, and the clearly different energy dependence for each one of such vibrational states was easily measured.

Let us start by considering a single intermediate vibronic state coupled to the partial waves describing the ionization of the valence shell leaving the ion in a specific vibrational state. By this model, we will not take into account, of course, any vibrational/lifetime interference, but the interference of the direct and the resonant photoemission path will be properly treated.[47] The photoemission from the $1b_1$ orbital, with contributions from $1b_1^{-1} \rightarrow \varepsilon_{a_1}$ (direct), $1b_1^{-1} \rightarrow \varepsilon_{b_1}$ (direct), $1b_1^{-1} \rightarrow \varepsilon_{a_2}$ (direct+resonant), is considered explicitly in this model, while an "effective" linewidth of the resonance is obtained by the coupling to an effective continuum representing all the other possible decay paths. The results of the K-matrix calculations for this model are collected in Fig. 7, where, as well as in the other figures mentioned in the following, the full line gives the photoabsorption cross section (arbitrary units), the dotted line gives the $1b_1^{-1}$ photoemission cross section (arbitrary units) and the heavy full line gives the $1b_1^{-1}\beta$ parameter as a function of photon energy. The relative photon energy is defined taking the lowest-lying resonance as origin.

Results of calculations using different values of F_{ij}^{rf} ("p" means positive, "n" negative, and 2 indicates a doubled value) are presented for comparison, as discussed in the following. As mentioned before, calculations have been done for the O $1s \rightarrow 2b_2$ core-excited state. However, the absolute energy of the resonance is not relevant in the following discussion and its value has been taken as energy origin in the present and in the following figures. It is quite clear, from the top-left (p) graph in Fig. 7 that the presence of the resonance leads to a strong dependence of β on the photon energy, with a clear asymmetry with respect to the absorption profile. A

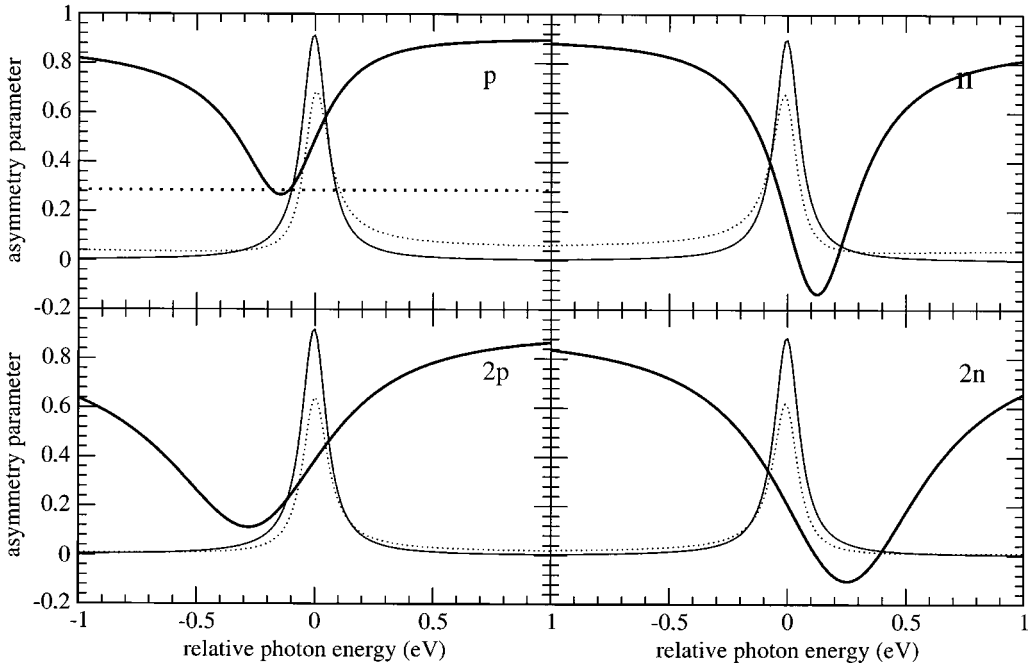

FIG. 7. Results of the K-matrix calculations. The full line gives the photoabsorption cross section (arbitrary units), the dotted line gives the $1b_1^{-1}$ photoemission cross section (arbitrary units), and the heavy full line gives the $1b_1^{-1}\beta$ parameter as a function of photon energy. In the different panels "p" stays for "positive," "n" stays for "negative," and "2" indicates a doubled value for the overlap between the vibrational wave functions of the resonant state and of the final state. The relative photon energy is defined taking the lowest-lying resonance as origin.

minimum of β appears on the low energy side where the negative interference of direct and resonant amplitudes occurs; this interference gives rise also to an asymmetry of the photoemission profile (dotted line) that is, however, hardly visible in the figure. The result of the calculations of β with the proposed one-step model confirm that, as well as it was found for the ionization branching ratios[47] in "participator" Auger decay of a molecular core resonance, also the anisotropy parameter shows a strong energy dependence for relatively large detuning from the resonance, due to a different resonant, or not resonant, behavior of the different partial wave amplitudes[49] contributing to β. As in the case of the branching ratios, it is the presence of a ratio of partial wave amplitudes in the expression of β,[49] which makes the interference between direct and resonant channels, that hardly affects the photoemission profile and it is practically negligible in the absorption profile, so important for the electron angular distribution. The details of the dependence of β from the photon energy around the resonance and, in particular, the position of the minimum depend, of course, on the molecular quantities entering in the expression of the direct amplitude [Eq. (5)] and of the resonant amplitude [Eq. (8)]. Even considering a single vibronic resonant state ($i=1$) as in the present case, a dependence from the character of the final vibronic state through the factor F_{1j}^{rf} remains. If the value of this factor is doubled we obtain the results presented in the bottom-left (2p) graph of Fig. 7 where β shows a deeper minimum shifted to lower energy. Depending on the actual "shape" of $|\chi_j^f\rangle$, which can be rather complex in a polyatomic molecule, the sign of F_{ij}^{rf} can also change sign for different j. Adopting for F_{ij}^{rf} the same value used for the results shown in the top-left (p) graph of Fig. 7, but with the opposite sign, we get the results shown in the top-left graph of Fig. 7. In this case β shows a minimum on the high energy side of the resonance, in agreement with a negative interference occurring now on that side.

The effect is emphasized by using a doubled negative value (2n) for F_{ij}^{rf}. In all the graphs we considered so far, β shows a sharp variation through the resonance band, either increasing or decreasing with the photon energy. A more complex behavior is obtained when the absorption band is formed by a number of peaks corresponding to different resonant vibronic states, due to the additional interference occurring among the resonant vibronic peaks. In order to add this vibrational/lifetime interference effect to our theoretical model, we extended it to two resonant vibronic states ($r,i=1,2$) of different intensity ($F_{01}^{gr}=0.9, F_{02}^{gr}=0.7$) and shifted in energy of about 0.2 eV. The results of this calculation, using for both F_{1j}^{rf} and F_{2j}^{rf} the same absolute value of the vibrational factor employed in the calculation shown in the top panels of Fig. 7, are displayed in Fig. 8. The four graphs (pp,np,pn,nn) refer to the different sign combinations that can be, in principle, realized for these two vibrational factors, depending on the shape of the $|\chi_j^f\rangle$ wave function considered. The four graphs show β profiles more complex than the one obtained for a single resonant state and that can be compared to the ones measured for the $1b_1^{-1}$ channel through the O $1s\rightarrow 2b_2$ band of H_2O. In particular the most peculiar profiles measured for the B and D final state bands (Fig. 5) seem to correlate quite reasonably to the computed profiles *np* and *pn*, respectively.

The electronic structure of the $1b_2^{-1}\,{}^2B_2$ final state has previously been discussed using two different models.[53] In one model, the state is assumed to be predissociated by two repulsive states $^4A''$ and $^2A''$.[54,34] In the other model a conical

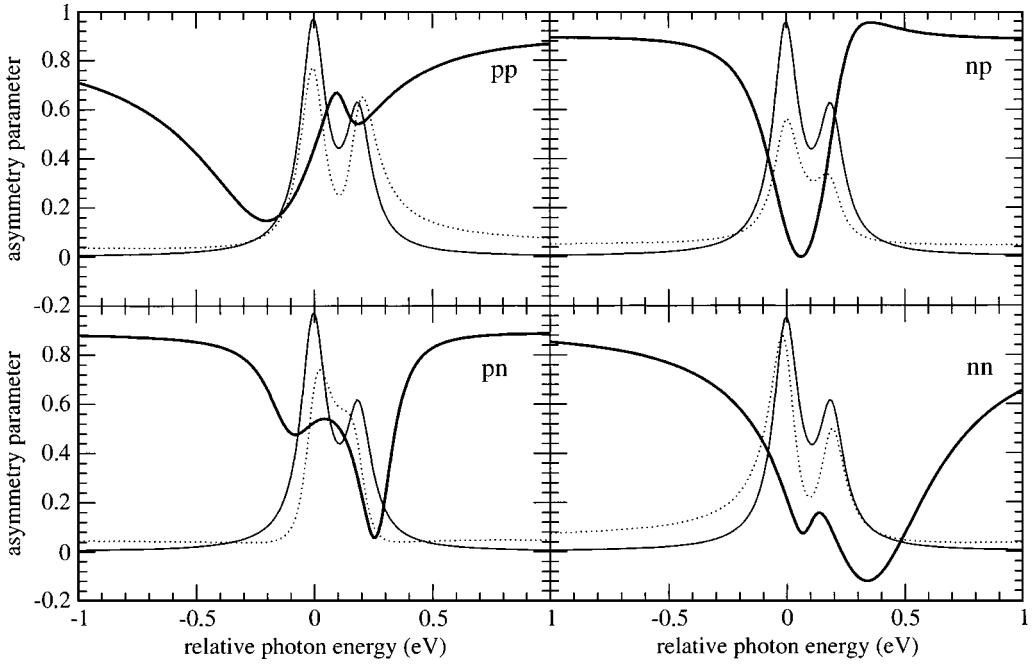

FIG. 8. Results of the K-matrix calculations extended to two resonant vibronic states. The full line gives the photoabsorption cross section (arbitrary units), the dotted line gives the $1b_1^{-1}$ photoemission cross section (arbitrary units), and the heavy full line gives the $1b_1^{-1}\beta$ parameter as a function of photon energy. In the different panels again p stays for positive and n stays for negative value for the overlap between the vibrational wave functions of the resonant state and of the final state. The four graphs (pp,np,pn,nn) refer to the different sign combinations that can be realized for the two vibrational factors corresponding to the two resonant vibronic states. The relative photon energy is defined taking the lowest-lying resonance as origin.

curve crossing is suggested between the $^2B_2$ and $^2A_1$ final states.[55] Previous UV-photoelectron measurements at higher resolution such as those reported in Refs. 40 and 53 show a distinct vibrational structure at binding energies below 18 eV, whereas at higher binding energies the structure merges into a complex set of broad peaks. This could be indicative of the lifetime broadening that occurs for short-lived dissociative states as suggested in the first model. However, several reports find that this model is inadequate to explain many observations[53,55,56] and therefore rather favor the second model involving a conical curve crossing with the $^2A_1$ state via excitation of the v_2 symmetric bending. Such a crossing over into the $^2A_1$ state could explain the large change of the β parameter and suggests that the curve crossing takes place around 18 eV.

The less clear picture of the energy dependence of β obtained in the case of the $1b_2^{-1}$ channel (Fig. 6) can be reasonably ascribed to the partial dissociative character of the $^2B_2$ state that does not allow a resolution of the individual vibrational final states. However, it should be pointed out that the proposed theoretical one-step model, although at present focused on the analysis of the observed energy dependence of β in the region of the O $1s \rightarrow 2b_2$ resonance, has a general validity for the description of the "participator" Auger angular distribution. In fact, it can be observed that also the experimental results for β of the $1b_2^{-1}$ channel in Fig. 6, that may, at first sight, appear different from those of the $1b_1^{-1}$ channel in Fig. 5, can be possibly rationalized by the proposed theoretical model and it can be said that the character of the modulation of β with the photon energy is, in reality, not so different from the one observed for the $1b_1^{-1}$ channel.

VI. CONCLUSION

We have measured the angular distribution of the first four resolved vibrational components of the $1b_1^{-1}$ state reached after resonant Auger decay of the O $1s \rightarrow 4a_1$ and the O $1s \rightarrow 2b_2$ core excitations and the trend of the angular distribution of different portions of the vibrational envelope of the $1b_2^{-1}$ state reached after resonant Auger decay of the O $1s \rightarrow 2b_2$ core excitation in water. We observe a strong variation on the angular distribution of emitted electrons as a function of which vibrational final states are reached after resonant Auger decay for both the $1b_1^{-1}$ and the $1b_2^{-1}$ states in core-excited water. For the $1b_1^{-1}$ state the most striking result is a large relative spread in the angular distribution parameter values for the first four single vibrational components across both resonances. For the $1b_2^{-1}$ state, the different trend in the angular distribution for different portions of the vibrational envelope can be, at first, ascribed to the dissociative nature of this final state above 18 eV binding energy.

We have shown that the extension of the model usually applied to describe normal Auger angular distributions to our resonant Auger case, based on a two-step description of the process,[29] fails to explain the observed excitation energy dependence of β. We have then proposed a more realistic one-step picture of the resonant photoemission process, including both vibrational/lifetime interference and interference between direct and resonant path, for the calculation of the photoelectron angular distribution. Since the quantitative agreement is not very informative and would require extensive and time-consuming calculations, we have presented a numerical simulation, based on the K-matrix approach and, partially, on *ab initio* calculations of the relevant molecular

quantities, of β for the $1b_1^{-1}$ decay channel of the O 1s $\rightarrow 2b_2$ resonance only, where the experimental data show a more clear dependence from the photon energy detuning.

From the comparison of experimental and theoretical results we conclude that the observed strong vibrational final state dependence of β for valence photoemission close to the core-excited states of H_2O can be ascribed to a mixing of vibrational/lifetime interference and interference between direct and resonant photoemission. The relative sign of the coupling between discrete resonant states and continuum final states, modulated by the overlap between the vibrational wave functions, gives origin to different trends of the energy dependence for different final vibrational states.

ACKNOWLEDGMENTS

This experiment was carried out with the approval of the SPring-8 program advisory committee. The authors are grateful to the staff at SPring-8 for their help. This work was supported in part by Grants-in-Aid for Scientific Research from the Japan Society for the Promotion of Science (JSPS) and by Grants-in-Aid for Scientific Research on Priority Area (B), Manipulation of Atoms and Molecules by Electronic Excitation. A.D. is grateful to JSPS for financial support during his stay in Sendai. V.C. is grateful for the hospitality of N. Kosugi at the Institute of Molecular Science in Okazaki (Japan) where part of the theoretical work was undertaken. The Swedish Research Council (VR) is gratefully acknowledged for economic support as well as the Swedish Foundation for Strategic Research (SSF).

[1] V. Schmidt, Rep. Prog. Phys. **55**, 1483 (1992).
[2] J. L. Dehmer, D. Dill, and A. C. Parr, in *Photophysics and Photochemistry in the Vacuum Ultraviolet*, edited by S. McGlynn, G. Findly, and R. Huebner (Reidel, Dordrecht, 1985), p. 341.
[3] U. Hergenhahn, J. Phys. B **37**, R89 (2004).
[4] G. B. Armen, H. Aksela, T. Åberg, and S. Aksela, J. Phys. B **33**, R49 (2000).
[5] N. Kabachnik and K. Ueda, Phys. Scr. (in press).
[6] O. Nayandin, E. Kukk, A. A. Wills, B. Langer, J. D. Bozek, S. Canton-Rogan, M. Wiedenhoeft, D. Cubaynes, and N. Berrah, Phys. Rev. A **63**, 062719 (2001).
[7] O. Hemmers, F. Heiser, J. Eiben, R. Wehlitz, and U. Becker, Phys. Rev. Lett. **71**, 987 (1993).
[8] U. Hergenhahn and U. Becker, J. Electron Spectrosc. Relat. Phenom. **72**, 243 (1995).
[9] E. Kukk, A. Wills, N. Berrah *et al.*, Phys. Rev. A **57**, R1485 (1998).
[10] A. Kivimäki, M. Neeb, B. Kempgens, H. M. Köppe, and A. M. Bradshaw, Phys. Rev. A **54**, 2137 (1996).
[11] E. Kukk, J. D. Bozek, W.-T. Cheng, R. F. Fink, A. A. Wills, and N. Berrah, J. Chem. Phys. **111**, 9642 (1999).
[12] O. Hemmers, F. Heiser, J. Viefhaus, K. Wieliczek, and U. Becker, J. Phys. B **32**, 3769 (1999).
[13] B. Wannberg, D. Nordfors, K. L. Tan, L. Karlsson, and L. Mattsson, J. Electron Spectrosc. Relat. Phenom. **47**, 147 (1988).
[14] K. Ueda, J. B. West, M. A. Hayes, M. R.F. Siggel, A. C. Parr, and J. L. Dehmer, J. Phys. B **26**, L601 (1993).
[15] K. Ohmori, H. Chiba, K. Amano, K. Ueda, Y. Sato, J. B. West, K. J. Ross, and M. Aymar, J. Phys. B **32**, 5223 (1999).
[16] N. Berrah, B. Langer, A. A. Wills, E. Kukk, J. D. Bozek, A. Farhat, and T. W. Gorczyca, J. Electron Spectrosc. Relat. Phenom. **101-103**, 1 (1999).
[17] A. C. Parr, J. B. West, M. R.F. King, K. Ueda, P. M. Dehmer, and J. L. Dehmer, J. Res. Natl. Inst. Stand. Technol. **106**, 795 (2001), and references therein.
[18] U. Fano, Phys. Rev. **124**, 1866 (1961).
[19] N. M. Kabachnik and I. P. Sazhina, J. Phys. B **9**, 1681 (1976).
[20] A. F. Starace, Phys. Rev. A **16**, 231 (1977).
[21] T. Carlson, D. Mullins, C. Beall, B. Yates, J. Taylor, D. Lindle, B. P. Pullen, and F. Grimm, Phys. Rev. Lett. **14**, 1382 (1988).
[22] K. Ueda, N. M. Kabachnik, M. Kitajima, M. Okamoto, Y. Shimizu, H. Chiba, T. Hayaishi, and H. Tanaka, J. Phys. B **33**, L475 (2000).
[23] A. De Fanis, N. Saito, M. Kitajima, Y. Shimizu, K. Okada, H. Tanaka, I. Koyano, and K. Ueda, J. Phys. B **34**, L377 (2001).
[24] H. Aksela, J. Jauhiainen, E. Nommiste, O.-P. Sairanen, J. Karvonen, E. Kukk, and S. Aksela, Phys. Rev. A **54**, 2874 (1996).
[25] K. Ueda, Y. Shimizu, H. Chiba, M. Kitajima, H. Tanaka, S. Fritzsche, and N. M. Kabachnik, J. Phys. B **34**, 107 (2001).
[26] M. Kitajima, M. Okamoto, Y. Shimizu *et al.*, J. Phys. B **34**, 3829 (2001).
[27] M. Kitajima, M. Okamoto, M. Hoshino *et al.*, J. Phys. B **35**, 3327 (2002).
[28] S. B. Whitfield, U. Hergenhahn, N. M. Kabachnik, B. Langer, J. Tulkki, and U. Becker, Phys. Rev. A **50**, R3569 (1994).
[29] K. Ueda, J. B. West, N. M. Kabachnik, Y. Sato, K. J. Ross, H.-J. Beyer, H. Hamdy, and H. Kleinpoppen, Phys. Rev. A **54**, 490 (1996).
[30] A. Kivimäki, M. Neeb, B. Kempgens, H. M. Köppe, K. Maier, and A. M. Bradshaw, J. Phys. B **30**, 4279 (1997).
[31] A. Kivimäki, E. Kukk, J. Karvonen, J. Mursu, E. Nommiste, H. Aksela, and S. Aksela, Phys. Rev. A **57**, 2724 (1998).
[32] I. Hjelte, M. N. Piancastelli, R. F. Fink *et al.*, Chem. Phys. Lett. **334**, 151 (2001).
[33] A. Hiraya, K. Nobusada, M. Simon *et al.*, Phys. Rev. A **63**, 042705 (2001).
[34] F. Fiquet-Fayard and P. M. Guyon, Mol. Phys. **11**, 17 (1966).
[35] H. Ohashi, E. Ishiguro, Y. Tamenori, H. Kishimoto, M. Tanaka, M. Irie, and T. Ishikawa, Nucl. Instrum. Methods Phys. Res. A **467**, 533 (2001).
[36] T. Tanaka and H. Kitamura, J. Synchrotron Radiat. **3**, 47 (1996).
[37] Y. Tamenori, H. Ohashi, E. Ishiguro, and T. Ishikawa, Rev. Sci. Instrum. **73**, 1588 (2002).
[38] H. Yoshida, Y. Senba, M. Morita *et al.*, AIP series of conference proceedings for SRI2003 (unpublished).
[39] N. Saito, K. Ueda, M. Simon *et al.*, Phys. Rev. A **62**, 042503 (2000).
[40] L. Karlsson, L. Mattsson, R. Jadrny, R. G. Albridge, S. Pinchas, T. Bergmark, and K. Siegbahn, J. Chem. Phys. **62**, 4745 (1975).
[41] T. R. Huet, C. J. Pursell, W. C. Ho, B. M. Dinelli, and T. Oka, J. Chem. Phys. **97**, 5977 (1992).
[42] D. Dill, J. R. Swanson, S. Wallace, and J. L. Dehmer, Phys. Rev. Lett. **45**, 1393 (1980).
[43] N. Saito, N. M. Kabachnik, Y. Shimizu, H. Yoshida, H. Ohashi, Y. Tamenori, I. H. Suzuki, and K. Ueda, J. Phys. B **33**, L729 (2000).
[44] A. De Fanis, N. Saito, H. Yoshida, Y. Senba, Y. Tamenori, H. Ohashi, H. Tanaka, and K. Ueda, Phys. Rev. Lett. **89**, 243001 (2002).
[45] R. Camilloni, M. Zitnik, C. Comicioli *et al.*, Phys. Rev. Lett. **77**, 2646 (1996).
[46] R. R.T. Marinho, O. Björneholm, S. L. Sorensen, I. Hjelte, S. Sundin, M. Bässler, S. Svensson, and A. Naves de Brito, Phys. Rev. A **63**, 032514 (2001).
[47] V. Carravetta, F. Kh. Gel'mukhanov, H. Ågren *et al.*, Phys. Rev. A **56**, 4665 (1997).
[48] V. Carravetta and H. Ågren, Chem. Phys. Lett. **354**, 100 (2002).
[49] I. Cacelli, V. Carravetta, A. Rizzo, and R. Moccia, Phys. Rep. **205**, 283 (1991).
[50] I. Cacelli and V. Carravetta, Chem. Phys. **243**, 77 (1999).
[51] V. Carravetta and H. Ågren, Phys. Rev. A **35**, 1022 (1987).
[52] V. Carravetta, H. Ågren, O. Vahtras, and H.J.A. Jensen, J. Chem. Phys. **113**, 7790 (2000).
[53] J. E. Reutt, L. S. Wang, Y. T. Lee, and D. A. Shirley, J. Chem. Phys. **85**, 6928 (1986).
[54] A. J. Lorquet and J. C. Lorquet, Chem. Phys. **4**, 353 (1974).
[55] J.H.D. Eland, Chem. Phys. **11**, 41 (1975).
[56] D. Dehareng, X. Chapuisat, J. C. Lorquet, C. Galloy, and G. Raseev, J. Chem. Phys. **78**, 1246 (1983).